Full paper

New Phytologist

Leaf surface water, not plant water stress, drives diurnal variation in tropical forest canopy water content

Xiangtao Xu[1,2], Alexandra G. Konings[3], Marcos Longo[4], Andrew Feldman[5], Liang Xu[4], Sassan Saatchi[4,6], Donghai Wu[2], Jin Wu[7] and Paul Moorcroft[1]

[1]Department of Organismic and Evolutionary Biology, Harvard University, Cambridge MA 02138, USA; [2]Department of Ecology and Evolutionary Biology, Cornell University, Ithaca NY 14850, USA; [3]Department of Earth System Science, Stanford University, Stanford CA 94305, USA; [4]Jet Propulsion Laboratory, California Institute of Technology, Pasadena CA 91109, USA; [5]Department of Civil and Environmental Engineering, Massachusetts Institute of Technology, Cambridge MA 02139, USA; [6]Institute of Environment and Sustainability, University of California, Los Angeles CA 90024, USA; [7]School of Biological Sciences, University of Hong Kong, Hong Kong China

Authors for correspondence:
Xiangtao Xu
Email: xx286@cornell.edu

Paul Moorcroft
Email: paul_moorcroft@harvard.edu

Received: *12 October 2020*
Accepted: *27 January 2021*

New Phytologist (2021) **231:** 122–136
doi: 10.1111/nph.17254

Key words: canopy water content (CWC), ecosystem modeling, ED2, leaf surface water, vegetation optical depth (VOD), X-band.

Summary

- Variation in canopy water content (CWC) that can be detected from microwave remote sensing of vegetation optical depth (VOD) has been proposed as an important measure of vegetation water stress. However, the contribution of leaf surface water (LW_s), arising from dew formation and rainfall interception, to CWC is largely unknown, particularly in tropical forests and other high-humidity ecosystems.
- We compared VOD data from the Advanced Microwave Scanning Radiometer for the Earth Observing System (AMSR-E) and CWC predicted by a plant hydrodynamics model at four tropical sites in Brazil spanning a rainfall gradient. We assessed how LW_s influenced the relationship between VOD and CWC.
- The analysis indicates that while CWC is strongly correlated with VOD ($R^2 = 0.62$ across all sites), LW_s accounts for 61–76% of the diurnal variation in CWC despite being < 10% of CWC. Ignoring LW_s weakens the near-linear relationship between CWC and VOD and reduces the consistency in diurnal variation. The contribution of LW_s to CWC variation, however, decreases at longer, seasonal to inter-annual, time scales.
- Our results demonstrate that diurnal patterns of dew formation and rainfall interception can be an important driver of diurnal variation in CWC and VOD over tropical ecosystems and therefore should be accounted for when inferring plant diurnal water stress from VOD measurements.

Introduction

Climate change and the accompanying intensification of hydrological cycles are imposing strong and chronic stress on terrestrial ecosystems (Novick *et al.*, 2016; McDowell *et al.*, 2018). Enhancing our understanding of vegetation water dynamics is therefore critical to predictions of ecosystem sensitivity to global change (Fatichi *et al.*, 2016; Schimel & Schneider, 2019). Recent work has shown that vegetation optical depth (VOD) estimated from microwave remote sensing observations is a reliable proxy for the canopy water content (CWC) and a promising source of data for monitoring and understanding vegetation water dynamics (Konings *et al.*, 2019; Feldman *et al.*, 2020). Changes in VOD can reflect vegetation diurnal water stress patterns (Konings & Gentine, 2017; Li *et al.*, 2017; Anderegg *et al.*, 2018; Zhang *et al.*, 2019), seasonality in plant water potential and leaf area (Guan *et al.*, 2014; Momen *et al.*, 2017), and vegetation biomass changes at longer time scales (Liu *et al.*, 2015; Fan *et al.*, 2019). However, accurate and robust interpretation of VOD variability remains challenging because of the complex physiological and biophysical processes impacting vegetation water dynamics at a wide range of time scales (Grossiord *et al.*, 2017). Variation in VOD can be driven by canopy water interception due to rainfall and dew formation, plant hydraulics, phenology, and structural changes from growth and mortality (Konings *et al.*, 2019). These challenges have hindered direct use of VOD in understanding vegetation water dynamics.

Spatio-temporal variation in VOD has mostly been linked to changes in leaf and wood internal water (WW_i) content (Jackson & Schmugge, 1991; Cosh *et al.*, 2010; Tian *et al.*, 2016), but theoretically they are also sensitive to surface water arising from dew formation and intercepted rainfall. While a previous study at a temperate agricultural site found relatively little effect of dew on airborne X-band (10.7 GHz) measurements (Du *et al.*, 2012), diurnal changes in leaf surface water (LW_s) were found to modulate tower-based VOD measurements collected at a similar microwave frequency (11.4 GHz) in a tropical canopy in Panama (Schneebeli *et al.*, 2011). The latter study was performed at the

scale of a few meters, however, which may show sensitivities not detectable at the ecosystem scale (Wigneron *et al.,* 2017).

At the ecosystem scale, the contribution of LW_s to VOD signals remains largely unknown despite LW_s being an important component of the moisture budget, particularly in rainforest ecosystems where significant diurnal and seasonal variation in CWC occurs because of frequent rainfall interception and dew formation (Junqueira Junior *et al.,* 2019; Binks *et al.,* 2021) and where measurements of LW_s beyond qualitative leaf wetness data (Binks *et al.* 2019) do not exist. Therefore, ignoring the contribution of LW_s to VOD can lead to overestimation of changes in leaf internal water (LW_i), which potentially biases the interpretation of VOD data as a measure of vegetation water stress. On the other hand, the ability to separate LW_s from CWC in VOD data may provide additional information about plant water dynamics. Through its effects on stomatal conductance, LW_s influences key aspects of plant metabolism, including carbon assimilation (Aparecido *et al.,* 2017; Gerlein-Safdi *et al.,* 2018a,b), and supports several important, yet relatively unknown, eco-physiological processes, such as leaf foliar water uptake (Eller *et al.,* 2013; Binks *et al.,* 2019) and epiphyte water use and survival (Lakatos *et al.,* 2012).

Recent advances in mechanistic representation of plant hydrodynamics in terrestrial biosphere models (Mencuccini *et al.,* 2019) provide a new avenue for the interpretation of VOD data: these models are now capable of explicit simulation of CWC dynamics from a set of biophysical descriptions and field-based plant functional traits. In turn, VOD data can provide valuable ecosystem scale evaluation data to hydrodynamic models, which are usually benchmarked by individual-level plant hydraulic measurements within forest plots (Christoffersen *et al.,* 2016; Xu *et al.,* 2016; Kennedy *et al.,* 2019; De Kauwe *et al.,* 2020). However, no studies to date have compared simulated CWC from terrestrial biosphere models with satellite VOD data.

In this study, we compare terrestrial biosphere model predictions of CWC with satellite VOD data, and quantify the contribution of LW_s to VOD variation across diurnal to seasonal and inter-annual time scales. Specifically, we make the following hypotheses: (H1) CWC, summed over the representative penetration depth of VOD observations, scales linearly with VOD; (H2) the contribution of LW_s to VOD is higher than leaf and wood internal water content (LW_i and WW_i) at the diurnal time scale because LW_s usually accumulates at night and evaporates during the day, while VOD at longer time scales is more likely controlled by changes in plant water stress and canopy biomass; (H3) the contribution of LW_s to VOD is higher at moist sites than at dry sites because there is more rainfall interception and dew formation under humid conditions.

To evaluate these hypotheses, we compare VOD data derived from X-band (10.7 GHz) measurements by the Advanced Microwave Scanning Radiometer for the Earth Observing System (AMSR-E) (Du *et al.,* 2017) to predictions of CWC from a terrestrial biosphere model incorporating plant hydrodynamics, at four tropical forest and savanna sites in Brazil across a large rainfall gradient. The AMSR-E VOD data covers full annual cycles from 2003 to 2010 and the satellite has local pass times of 01:30 h and 13:30 h that can reasonably capture diurnal changes (Konings & Gentine, 2017; Li *et al.,* 2017) in addition to seasonal and inter-annual variation in CWC. The terrestrial biosphere model used in this study is the Ecosystem Demography v.2 (ED2). It is an ideal model platform for the evaluation of the relationship between CWC and LW_s with VOD because the model explicitly incorporates plant hydraulics and leaf energy budget (Xu *et al.,* 2016; Longo *et al.,* 2019), enabling it to simulate the dynamics of LW_s, LW_i and WW_i, as well as their horizontal and within-canopy vertical heterogeneity.

Materials and Methods

Model description

Ecosystem Demography v.2 (Medvigy *et al.,* 2009) is an individual-based terrestrial biosphere model that represents the dynamics of structurally and functionally diverse plant canopies. The most recent version of the model (ED-2.2, Longo *et al.,* 2019) has explicit representation of the leaf water and energy budget at sub-hourly resolution for each plant cohort. The model calculates changes in LW_s for each plant cohort as the balance of dew formation, evaporation, rainfall interception, and water shedding. A detailed description of the water fluxes that contribute to the dynamics of LW_s in the model can be found in Supporting Information Notes S1.

Ecosystem Demography v.2 is also one of the first models to couple trait-based plant hydraulics with vegetation demographic dynamics (Xu *et al.,* 2016). The hydraulics-enabled version (ED2-hydro) separates plant internal water pools into leaf and stem water pools at the cohort level, and estimates sub-hourly water exchanges between these two pools using water potential gradient and cohort-specific stem water conductance following Darcy's law. The integration of plant hydraulics with stomatal conductance and rhizosphere water uptake enables cohort-level simulation of the dynamics of plant internal water content (see Notes S1 for details). ED2-hydro has been calibrated and evaluated in several neotropical forests across a large precipitation gradient (Xu *et al.,* 2016; Powell *et al.,* 2017, 2018).

In this study, we used the functionality of ED-2.2-hydro to conduct mechanistic simulations of all major components of vegetation CWC. We updated key plant hydraulic parameters for tropical plant functional types (PFTs) based on a meta-analysis over tropical species (Christoffersen *et al.,* 2016) to incorporate the effects of plant functional diversity. Since the vertical structure of vegetation biomass can influence the interpretation of VOD data due to the limited penetration depth of microwave signals (Chaparro *et al.,* 2019), we also made updates to allometry, trait phenoplasticity, and mortality within the model, to improve simulated vegetation structure in tropical forests (Notes S1). The model parameterization (Table S1) used in this study is archived at https://github.com/xiangtaoxu/ED2/tree/VOD.

Model configuration and simulation setup

We conducted simulations for two tropical moist forests (Manaus K34 and Reserva Jaru) that both receive > 2000 mm yr^{-1} mean

annual rainfall, and two tropical savanna sites (Brasília and Pé-de-Gigante) that both receive < 1500 mm yr^{-1} mean annual rainfall (Table 1). These sites were selected based on the quality of AMSR-E VOD data available for these locations (in particular, minimal contamination from nearby rivers or other large bodies of water) and the availability of *in-situ* meteorological data (Brasília: SONDA-INPE (2020); other sites: de Gonçalves *et al.* (2013)).

Since the temporal coverage of *in-situ* meteorological data ranges from 1999 to 2012 depending on the site (Table 1) but does not encompass the full length of the AMSR-E VOD time series (2003–2010), we integrated the ground measurements with climate reanalysis data from Modern-Era Retrospective analysis for Research and Applications v.2 (MERRA2) (Gelaro *et al.,* 2017). To avoid the known biases in MERRA2 precipitation data for tropical regions (Beck *et al.,* 2019), we used the Climate Hazards Group InfraRed Precipitation with Station (CHIRPS) precipitation data (Funk *et al.,* 2015). To minimize the systematic biases in the reanalysis meteorology relative to local climate, and to preserve monthly values, we calculated the difference between the monthly average of the reanalysis data and *in-situ* data for each variable over the years for which *in-situ* data is available. We then applied the difference to modify the whole reanalysis time series to obtain the meteorological forcing (Fig. S1). The difference for precipitation is in logarithm space, so that no rainfall was added to dry days when we applied the difference.

Simulations at each site consisted of a 400-yr model spin-up to attain steady state vegetation structure and composition followed by a 30-yr contemporary simulation (1981–2010) encompassing the AMSR-E measurements. For the spin-up simulation, we initialized the model with a small number of seedlings (0.1 individuals m^{-2}) of all four PFTs and ran the model with a cycling meteorological forcing from 1981 to 2000. Following up the spin-up simulations, we ran the model forced by meteorology from 1981 to 2010. For both sets of simulations, we used a constant rate of 1% of forest area experiencing windthrow disturbance (i.e 0.01 ha ha^{-1} yr^{-1}) and a constant atmospheric CO_2 of 380 ppm.

Vegetation optical depth retrievals

We used X-band (10.7 GHz) VOD retrieved from observations of the Japanese Aerospace Exploration Agency (JAXA) AMSR-E instrument. Specifically, the VOD data were those retrieved by the Land Parameter Data Record (LPDR) v.2 (Jones & Kimball, 2012; Du *et al.,* 2017). The LPDR uses a multi-step procedure to disentangle the contributions of VOD, vegetation scattering, soil moisture, temperature, atmospheric humidity, and open water bodies to the observed radiometric brightness temperatures (Jones *et al.,* 2010).

Although the Amazon rainforest remains among the most challenging ecosystems for accurate VOD retrieval due to the large heterogeneity in canopy structure and the associated biophysical properties, interpretation of microwave radiometry has proven feasible even in highly complex canopies: for example, Calvet *et al.* (1994) used a site-specific model to determine the relationship between Ka-band radiometry and stomatal resistance at Manaus. Nevertheless, the VOD retrievals are expected to be more accurate at the savanna sites than at the densely forested sites.

Model evaluation and comparison with VOD

We first evaluated the terrestrial biosphere model's predictions of vegetation structure and plant hydraulics because both of these characteristics directly affect CWC. We compared vertical profiles of leaf area index (LAI) derived from the Geoscience Laser Altimeter System (GLAS) aboard the Ice, Cloud, and land Elevation Satellite (ICESat), which has previously been shown to capture variation in tropical forest structure (Tang & Dubayah, 2017; Yang *et al.,* 2018), with model-simulated LAI profiles. Site-specific LAI profiles were derived from GLAS waveforms using a light-extinction model based on the MacArthur & Horn (1969) approach (Ni-Meister *et al.,* 2001; Tang *et al.,* 2014) using measurements collected between 2003 to 2008 (Zwally *et al.,* 2014) within a 50-km grid box centered around each study site. We extracted simulated average LAI profiles using model outputs from the same period of time for comparison. Both the GLAS and simulated LAI profiles were aggregated to a vertical resolution of 5 m. Leaf area index can show large seasonal changes, especially at the two savanna sites. Therefore, we also compared the average seasonality of total LAI with the Moderate Resolution Imaging Spectroradiometer (MODIS) LAI data (Didan, 2015).

In contrast to the availability of measurement data for vegetation structure, there are no high-resolution long-term

Table 1 Description of climate and soil conditions used for ED-2.2-hydro simulations at the four study sites.

Site name	Location (lat. long.)	MAT[1] (°C)	MAP (mm)	Soil texture (% of sand and clay)[2]	Temporal coverage of *in situ* meteorology[3]
Manaus K34 (M34)	−2°37′, −60°13′	25.7	2673	20, 68	1999–2006
Reserva Jaru (RJA)	−10°5′, −61°56′	25.0	2069	80, 10	1999–2002
Pé-de-Gigante (PDG)	−21°37′, −47°39′	22.8	1453	85, 3	2001–2003
Brasília (BSB)	−15°36′, −47°43′	21.7	1344	13, 53	2010–2012

[1]MAT, mean annual temperature; MAP, mean annual precipitation.
[2]We used the best estimates of soil texture following previous ED2 simulations (Longo, 2014; Restrepo-Coupe *et al.,* 2017), and the same soil depth of 10 m.
[3]Meteorological variables necessary to drive the model include incoming shortwave and longwave radiation, temperature, humidity, pressure, precipitation, and wind speed.

measurement data for plant hydraulic properties (e.g. leaf water potential) over tropical forests. Limited field measurements suggest leaf water potential for tropical canopy trees normally varies between 0 and −1 MPa within a day at moist sites (Fontes *et al.,* 2018) and can drop below −2 MPa at seasonally dry forest (Wu *et al.,* 2020) and Cerrado sites (Bucci *et al.,* 2005). We therefore tested whether the simulated diurnal variation showed a similar range of variation.

For LW_s, there are no direct measurement data for its diurnal and seasonal cycles in the tropics to the best of our knowledge. Limited measurements report predawn values for top canopy leaves ranging from 0.02 to 0.11 kg H_2O m^{-2} leaf in a tropical moist forest at Caxiuanã (O. Binks, pers. comm) and from 0.02 to 0.08 kg H_2O m^{-2} leaf for five species in a tropical moist forest in Costa Rica (Aparecido *et al.,* 2017). Our simulated LW_s at predawn (06:00 h) in top canopy leaves showed a consistent range at a similarly wet forest site and predicted that top canopy leaves are frequently wet at predawn (Fig. S2), which is consistent with a recent report at Caxiuanã using leaf wetness sensors (Binks *et al.,* 2021). Altogether, these consistencies suggest the model predictions on LW_s dynamics are realistic.

Following the model evaluation, we used daily AMSR-E VOD data for both 01:30 h and 13:30 h, and extracted the hourly average values of simulated LW_s, LW_i and WW_i, the three components of CWC in ED-2.2-hydro, for the same times as the VOD observations. We averaged both VOD and simulated CWC data into biweekly values to reduce high-frequency variation and noise in VOD (Konings *et al.,* 2016). In forests, X-band VOD is mostly sensitive to top canopy layers due to its high electromagnetic frequency (Macelloni *et al.,* 2001; Guglielmetti *et al.,* 2007). The depth at which significant canopy attenuation occurs, commonly referred to as the penetration depth, depends on both canopy structure and water status, and thus is variable in both space and in time. Spatial and temporal variation in penetration depth are generally not accounted for in retrieval algorithms (Konings *et al.,* 2016; Du *et al.,* 2017). Recently, Chaparro *et al* (2019) showed that X-band VOD values saturate when aboveground biomass (AGB) is higher than 1 kgC m^{-2}. Therefore, we chose a conservative average penetration depth by only including LW_s, LW_i, and WW_i for the top 1 kgC m^{-2} of biomass (leaf and wood, which corresponds to 2–10 m depending on forest biomass vertical profiles) for each forest patch within site-level simulation results (Fig. S3) when comparing simulated CWC and AMSR-E VOD. Additionally, we also evaluated how VOD and CWC relationships vary with different assumptions of penetration depth.

We conducted analyses using the corresponding VOD data and CWC simulations across diurnal and biweekly time scales. First, we extracted the predicted diurnal cycle of LW_s, LW_i, and WW_i to investigate the roles of each water pool in determining CWC dynamics that emerge from ED-2.2-hydro. Specifically, we derived the contributions of LW_s, LW_i and WW_i to the variations in total CWC from the model at both diurnal and biweekly time scales by calculating the fractional contributions of each sub-component variance to the total CWC variance. For the diurnal-scale analysis, we quantified the variance as the value difference between 01:30 h and 13:30 h, since there are only two VOD observations within each diurnal cycle. For the biweekly-scale analysis, we calculated the variance of the mean of the 01:30 h and 13:30 h data for each biweekly (14 d) period.

Second, we compared the VOD measurements and CWC data and assessed the role of LW_s in their relationships. To test our first hypothesis, on the scaling between VOD and CWC (H1), we quantified the linear relationship between VOD and CWC using ordinary least squares (OLS) regression for each site and all sites combined. To test our second and third hypothesis on the contribution of LW_s to CWC and VOD dynamics and its variation across sites (H2 and H3), we compared VOD and two metrics of CWC: (1) CWC_{int} that only includes the internal water content of leaf and wood; and (2) CWC_{all} that includes both leaf and WW_i and LW_s.

Specifically, we assessed the cross-site variation in isohydricity index, a widely-used metric to describe the diurnal behavior of plant water use (Martínez-Vilalta *et al.,* 2014; Konings & Gentine, 2017). This metric (σ) is calculated using the following regression equation:

$$X_{13:30\,h} = \sigma \times X_{01:30\,h} + \Lambda \qquad \text{Eqn 1}$$

where σ is the isohydricity index, Λ is the regression intercept, and X is a state variable describing canopy water status.

Low σ implies vegetation is more isohydric because daytime water status is relatively insensitive to nighttime water status due to stomatal control, while higher σ implies vegetation is more anisohydric. We calculated σ values for observed VOD, simulated CWC, and leaf water potential to investigate whether and how VOD-based isohydricity (generally assumed to reflect LW_i stress) is affected by LW_s dynamics.

We then contrasted the average seasonality and deseasonalized multi-year variation of VOD and simulated CWC for each study site in terms of both absolute values at 01:30 h and relative diurnal range ($100\% - X_{13:30\ h}/X_{01:30\ h} \times 100\%$). Together with variance decomposition of the simulated CWC, the evaluation of these two metrics enables quantification of the impacts of leaf and wood water content and LW_s on VOD.

Results

Predictions of vegetation structure and plant water potentials

The long-term model equilibrium yielded LAI profiles that were generally consistent with GLAS estimates at the four evaluation sites (Fig. 1a–d). Individual-level competition in the model led to a general demographic size structure of a few big trees and many small trees, yielding decreasing leaf area density (LAD) from forest understory to canopy top that largely falls into the uncertainty of LiDAR-based estimates. At the two forest sites (M34 and RJA), top canopy height reached 35–40 m, while LAD became very small (< 0.01 m^{-2} m^{-3}) above 20 m at the two savanna sites (PDG and BSB). However, the model tended to overestimate the total LAI at the sites by 0.3–0.5 m^2 m^{-2}

(Fig. 1a–d), with the excess LAI arising mainly from overestimates of LAD in upper canopy layers. The model simulations also tended to underestimate LAD in the lowest (< 5m) canopy layer at the two forest sites.

Seasonal changes in predawn leaf water potential govern the seasonal dynamics of canopy leaf phenology the model. As a result, seasonality of total leaf area was minimal at M34, where total rainfall is high and rainfall seasonality is mild. There were slight decreases in LAI at RJA (*c.* 0.2 m^2 m^{-2}), and larger (0.5–1 m^2 m^{-2}) decreases at PDG and BSB toward the end of the dry season (Fig. 1e–f). MODIS LAI exhibited qualitatively similar patterns of LAI seasonality between the wet and dry sites. However, at M34, the MODIS LAI estimates exhibit increases in LAI during the wet season, and earlier onset of leaf shedding around the start of the dry season at PDG and BSB, compared to the model simulations. Overall, ED-2.2-hydro generated canopy vertical structure and increasing seasonal magnitude in canopy phenology from wet sites to dry sites, a result that is largely consistent with remote sensing observations.

The biosphere model simulations imply significant spatio-temporal variation in leaf water potential (Ψ_{leaf}) across all four sites (Fig. 2). For upper canopy leaves, the average maximum Ψ_{leaf} was close to zero for wet sites and for the wet season at dry sites (Fig. 2e–f), implying a full recharge of daytime water loss in the model. In the dry season at PDG and BSB, maximum Ψ_{leaf} dropped below −1 MPa, triggering leaf shedding in the model. The daily minimum Ψ_{leaf} values for canopy leaves were generally 1–1.5 MPa lower than the maximum values, depending on moisture supply. These average patterns in leaf hydrodynamics are consistent with observed variation in leaf water potentials over tropical forests (Bucci *et al.*, 2005; Fontes *et al.*, 2018; Wu *et al.*, 2020). Wood water potential at the base of stems (Ψ_{stem}) had similar diurnal cycles and seasonality to Ψ_{leaf} (Fig. S4). However, the simulated Ψ_{stem} was always close to zero at M34, the wettest site in our study (Fig. S4a), whereas at the two drier sites ψ_{stem} showed reduced diurnal variation during the wet season (Fig. S4c-d), but similar seasonal variation to Ψ_{leaf}.

While observations of diurnal and seasonal variation in plant water potential were not available, the model's predictions of evapotranspiration (ET) matched observed patterns of ET seasonality that were available from flux tower measurements at M34, RJA, and PDG (Fig. S5), providing additional support for the model's ability to capture key characteristics of vegetation hydrodynamics at our study sites.

Spatio-temporal variation in simulated CWC and VOD observations

The model simulations indicate that LW_s dominates the diurnal cycles of CWC, despite constituting < 10% of the total CWC of the upper canopy layers on average (Fig. 3). Generally, LW_s accumulated from late afternoon, reached peak values in the early morning, then declined to near zero by midday. By contrast, LW_i varied by only 10–15% within a day, and WW_i showed even smaller diurnal variation (Fig. 3a–d). As a result, LW_s was shown to make a substantial contribution to CWC diurnal variability (Fig. 3e–h), accounting for 76% of CWC differences between 01:30 h and 13:30 h at M34 (the wettest site) and 61% at BSB (the driest site). Internal leaf water (LW_i) generally accounted for more of the remaining CWC diurnal variance than WW_i. At the

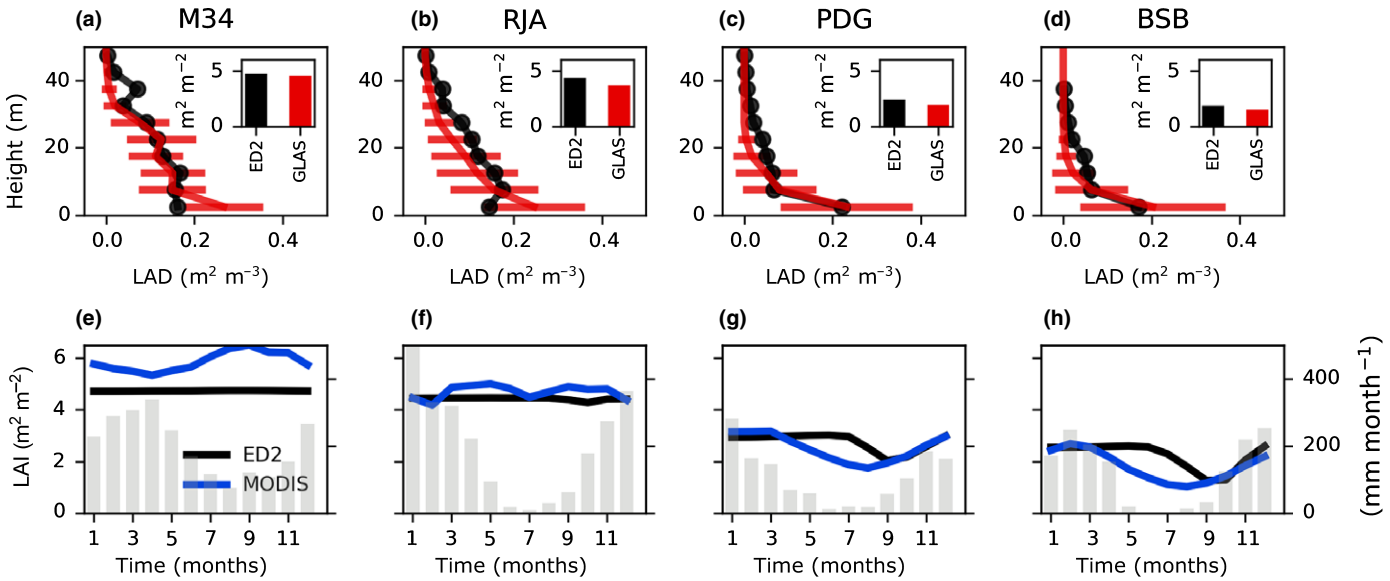

Fig. 1 Evaluation of vegetation structure in ED-2.2-hydro across four study sites along a rainfall gradient. (a–d) The average profile of leaf area index (LAI) within the forest canopy from the Geoscience Laser Altimeter System (GLAS) LiDAR inversion (red) and model simulations (black). Red error bars represent SD of GLAS data within the 50-km grid cell around each site. The *x*-axis represents leaf area density (LAD) for each 5-m band from 0 to 50 m above ground, while the *y*-axis represents the height of each band. Inset plots within each panel compare the total LAI from model and GLAS data. (e–h) Seasonality of monthly average canopy total LAI from model simulation (black) and observations from the Moderate Resolution Imaging Spectroradiometer (MODIS, blue). Grey bars denote the average monthly rainfall in mm. Each column displays results for a study site, with mean annual rainfall at the top of each column. M34, Manaus K34 site; RJA, Reserva Jaru site; PDG, Pé-de-Gigante; BSB, Brasília site.

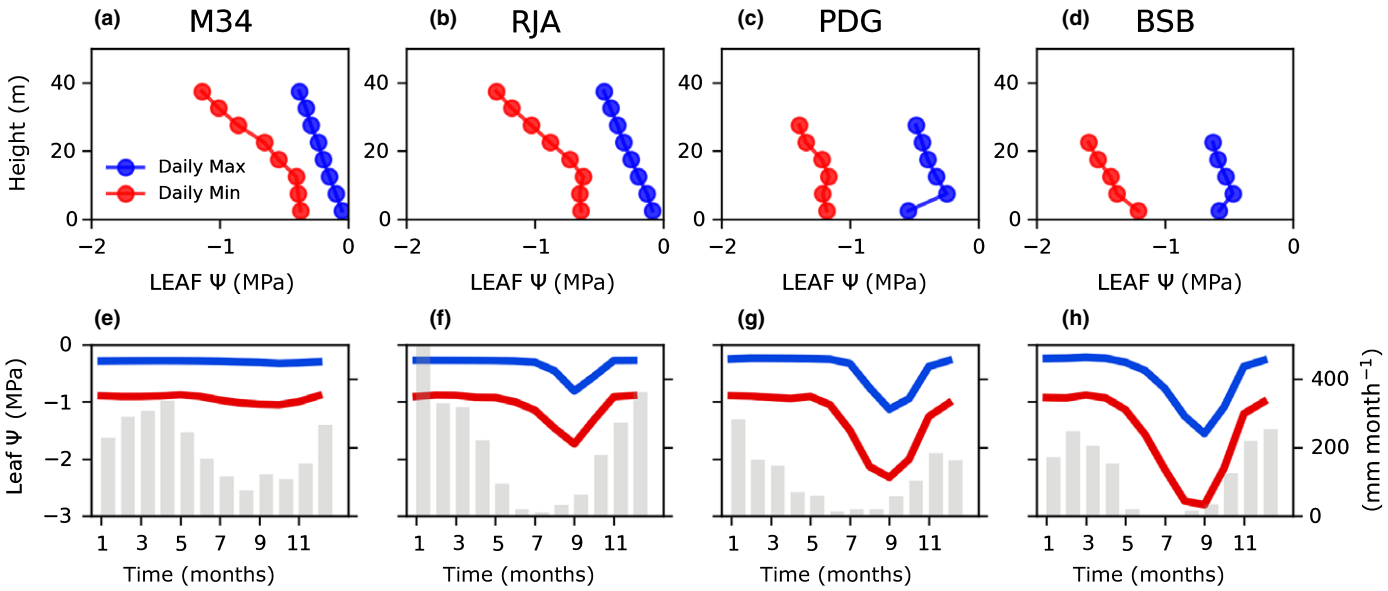

Fig. 2 Simulated leaf hydrodynamics in ED-2.2-hydro. (a–d) vertical distribution of daily maximum (blue) and minimum (red) leaf water potential. We averaged cohort-level leaf water potential for every 5-m height band, using cohort leaf area index as weighting factors. (e–h) seasonality of average daily maximum and minimum leaf water potential for upper canopy leaves. We define upper canopy as the top 1 kgC m^{-2} biomass. M34, Manaus K34 site; RJA, Reserva Jaru site; PDG, Pé-de-Gigante; BSB, Brasília site.

biweekly timescale, the contribution of LW_s was considerably lower (18–36% for RJA, PDG, and BSB), except for at M34, where LW_s still drove seasonal and inter-annual variations in the simulated CWC. In addition, at this time scale, WW_i became the dominant driver of CWC variation, except at the wettest site (M34). Increasing the penetration depth to 10 kgC m^{-2} of AGB did not qualitatively change these general cross-site and cross-time-scale patterns; it did however, increase the contribution of WW_i pools to patterns of diurnal and seasonal patterns of CWC variability (Fig. S6).

We found a strong linear relationship between VOD and simulated CWC_{all} (top 1 kgC m^{-2} of AGB) with an R^2 value of 0.62 (Fig. 4a). The relationship remained significant at site-level, but the R^2 and slope values varied: simulated CWC_{all} explained < 20% of variance in VOD at the two moist forest sites, M34 and RJA, but accounted for about 50% of variance at the two savanna sites, PDG and BSB (Fig. 4c,d). At the same time, the sensitivity of VOD to CWC_{all} (indicated by the slope of the VOD regressed against CWC_{all}) increased by *c.* 300% from the wettest site (M34; slope = 0.55) to the driest site (BSB; slope = 2.15), whereas the regression slope of data from all sites combined fell in between these values (slope = 0.86). The relationship between CWC_{int} (CWC excluding LW_s) and VOD was weaker (R^2 = 0.60 for all data combined) and the site-specific R^2 values declined by 5–10% for M34, BSB, and PDG, while RJA showed little change (Fig. 4b,c). The site-specific regression slopes of the VOD-CWC_{int} relationship all steepened due to the increasing nonlinearity of the relationship, while the cross-site variations did not change much (Fig. 4b). As a result, the VOD-CWC_{int} regression slope value using data from all sites combined (0.96, black line in Fig. 4) became lower than site-specific values (1.2–2.8, colored lines in Fig. 4). Using a much greater penetration depth that included the top 10 kgC m^{-2} of AGB yielded similarly high R^2 values (0.61 for both CWC_{all} and CWC_{int}), but the R^2 values were far lower than 0.1 for the two moist forest sites, and the cross-site regression slope value was much lower than all site-level regression slopes, regardless of whether or not LW_s was included (Fig. S7). Overall, the model predictions of CWC that included all forms of canopy water showed robust linear relationships with VOD, but the relationships were stronger at drier sites and across sites along a rainfall gradient.

We calculated isohydricity (σ) values from the variability in biweekly VOD estimates and calculated a similar metric from model simulations of biweekly variability in CWC_{all}, CWC_{int} and canopy Ψ_{leaf}. Our VOD-based isohydricity values were comparable to the values estimated by Konings & Gentine (2017) and Li *et al.* (2017) from daily VOD observations. As seen in Fig. 5(a–d), the VOD-based σ was low at the two wet sites (0.44 for M34 and 0.59 for RJA, respectively) and higher at two dry sites (0.71 for PDG and 0.72 for BSB, respectively). The largest difference between VOD-based and CWC_{all}-based isohydricity occurred at M34, where the simulated isohydricity was considerably lower than the VOD-derived estimate (σ = 0.18 and 0.44, respectively). However, the isohydricity values from the model predictions of CWC_{all} and VOD observations were very close at the other three sites (Fig. 5a–h). By contrast, dynamics of CWC_{int} and Ψ_{leaf} implied almost perfect to extreme anisohydric behavior across all sites with σ values very close to or larger than one (Fig. 5i–p), highlighting the significant contribution of LW_s to the diurnal variation in simulated CWC_{all}, and, by inference, to VOD measures of isohydricity.

We also compared the average seasonality of simulated CWC and observed VOD with respect to both their values at 01:30 h and their diurnal ranges (Fig. 6). At the two moist forest sites,

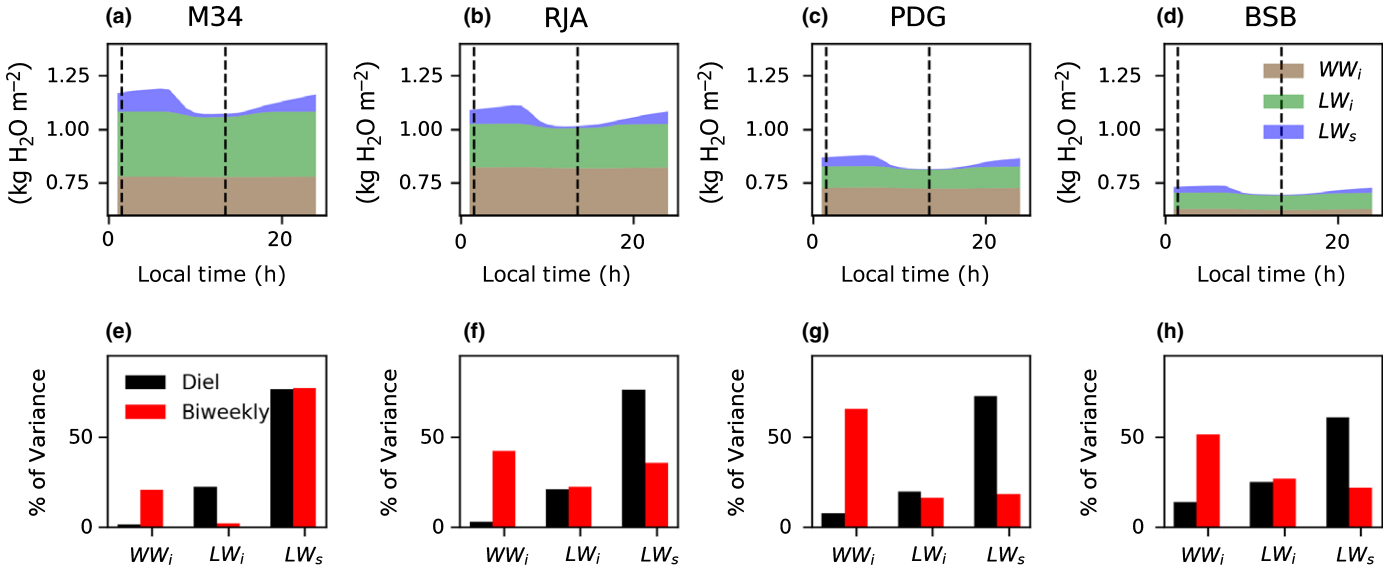

Fig. 3 Contribution of leaf surface water to canopy water content (CWC) in model simulations. (a–d) Average diurnal cycles of CWC partitioned into wood internal water (WW_i, brown), leaf internal water (LW_i, green), and leaf surface water (LW_s, blue) for our four study sites. The vertical dashed lines represent the local time of the satellite pass for vegetation optical depth (VOD) measurements (01:30 h and 13:30 h). (e–h) Variance decomposition of CWC temporal variations into the three sub-components at both the diurnal time scale (black bars) and biweekly time scale (red bars). We only used the simulated CWC at the same time as the VOD measurements (dashed lines in a–d) for this analysis. M34, Manaus K34 site; RJA, Reserva Jaru site; PDG, Pé-de-Gigante; BSB, Brasília site.

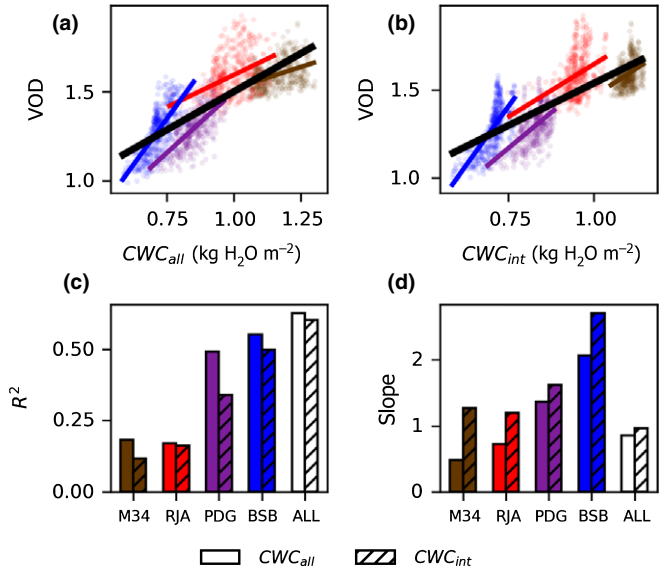

Fig. 4 Relationship between vegetation optical depth (VOD) and (a) simulated CWC_{all} (canopy water content including leaf surface water) and (b) CWC_{int} (canopy water content excluding leaf surface water). Each dot represents the biweekly average of 01:30 h or 13:30 h values, with the colors indicating the different study sites, M34 (brown), RJA (red), PDG (purple), and BSB (blue). Solid black lines represent ordinary least square linear regression between VOD and CWC using all data combined, while solid color lines represent regressions for each site. R^2 (c) and slope (d) values are also shown for each site and all sites combined. Only CWC dynamics from the top 1 kgC m^{-2} biomass are included in the simulations. M34, Manaus K34 site; RJA, Reserva Jaru site; PDG, Pé-de-Gigante; BSB, Brasília site.

01:30 h VOD showed seasonal patterns that peaked in the middle of the dry season, with a seasonal amplitude of *c.* 10% at M34 and 20% at RJA (black lines in Fig. 6a,b, respectively). Simulated CWC_{all} did not reproduce these patterns, however, showing minimal seasonality at M34 and a small and short decline in late dry season at RJA (green lines in Fig. 6a,b, respectively). At the two savanna sites, 01:30 h VOD showed 20–25% seasonal variation, peaking in the late wet season and reaching its lowest values in the late dry season (black lines in Fig. 6c,d, respectively). The simulated 01:30 h CWC_{all} showed similar seasonal patterns and amplitude (green lines in Fig. 6c,d, respectively). As a result, the correlation between VOD and simulated CWC_{all} increased from around zero at wet sites to *c.* 0.8 at the dry sites. Interestingly, CWC_{int}, which excludes the highly seasonal LW_s (varying by 30–100%) that follows the seasonality of rainfall (Fig. S8a–d), exhibited stronger correlation with VOD seasonality, particularly at the two wet sites (Pearson's *r* increased from approx. 0 to 0.4–0.5) but also a reduction in seasonal amplitude by 5–10% at all sites.

The comparison of the seasonality in the diurnal range showed similar patterns, with the model-data correlation increasing from wetter sites to drier sites (Fig. 6e–h). However, the influence of LW_s was more prominent at the savanna sites. At these two drier sites, the simulated diurnal range of CWC_{int} peaked in mid-to-late dry season when daytime atmospheric water demand was high and soil water supply was low. Inclusion of LW_s, whose diurnal range could reach 80–100% (Fig. S8e–h), resulted in shifts of the peak to late wet season for CWC_{all}, which is consistent with VOD seasonality, and led to comparable average diurnal range values (5–10%) to the VOD data. At the two forest sites, the inclusion of LW_s reduced the temporal correlation of the diurnal range between VOD and CWC_{all} for M34 and reversed the correlation for RJA; however, it increased the average diurnal range so that it was closer to the VOD observations. The

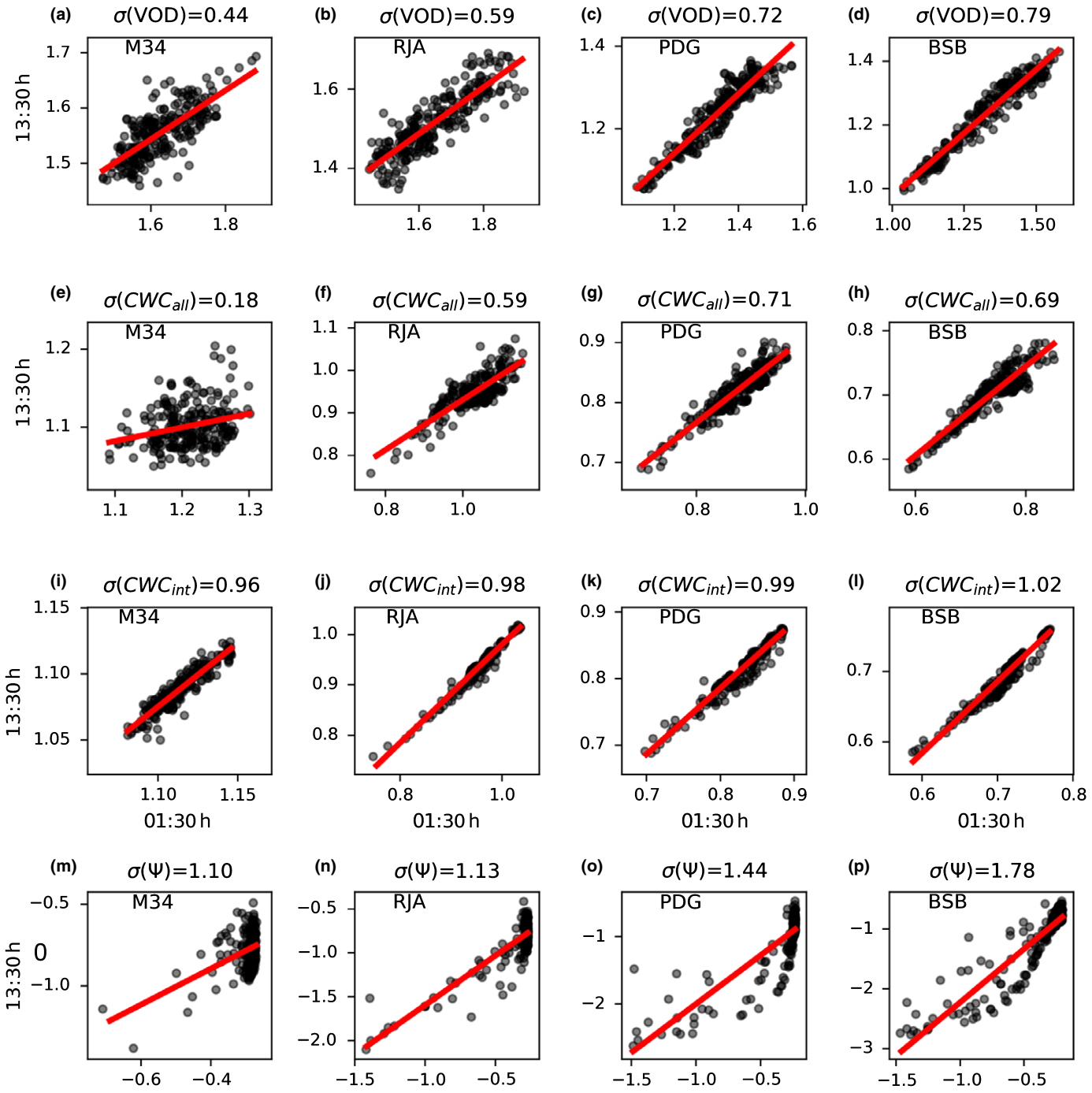

Fig. 5 Isohydricity index (σ) from vegetation optical depth (VOD, a–d), canopy water content including leaf surface water (CWC_{all}, e–h), CWC excluding leaf surface water (CWC_{int}, i–l), and leaf water potential (m–p, Ψ in MPa). Each column represents results from one study site. Each dot represents a biweekly average of VOD, CWC_{all}, CWC_{int} or Ψ. Canopy water content and Ψ values represent water content and average leaf water potential of the upper canopy layers (top 1 kgC m^{-2}). Red lines represent linear regression results, with σ values shown at the top of each panel. All regressions are significant. All regression slopes have a *P*-value lower than 0.05. M34, Manaus K34 site; RJA, Reserva Jaru site; PDG, Pé-de-Gigante; BSB, Brasília site.

model-predicted diurnal range may bias low because WW_i is calculated from water potential at the base of the stem, which may have smaller diurnal range than branch water potential in nature. A post-hoc correction made by assuming wood water potential is the same as leaf water potential increased the average diurnal range in CWC by 2–3% but did not change the seasonal patterns or the impact of LW_s (Fig. S9). Overall, these results suggest that ED-2.2-hydro did not capture the seasonality in canopy hydrodynamics and phenology at the forest sites; however, it performed well at the two savanna sites, where consideration of LW_s significantly improved the agreement between simulated CWC and VOD observations.

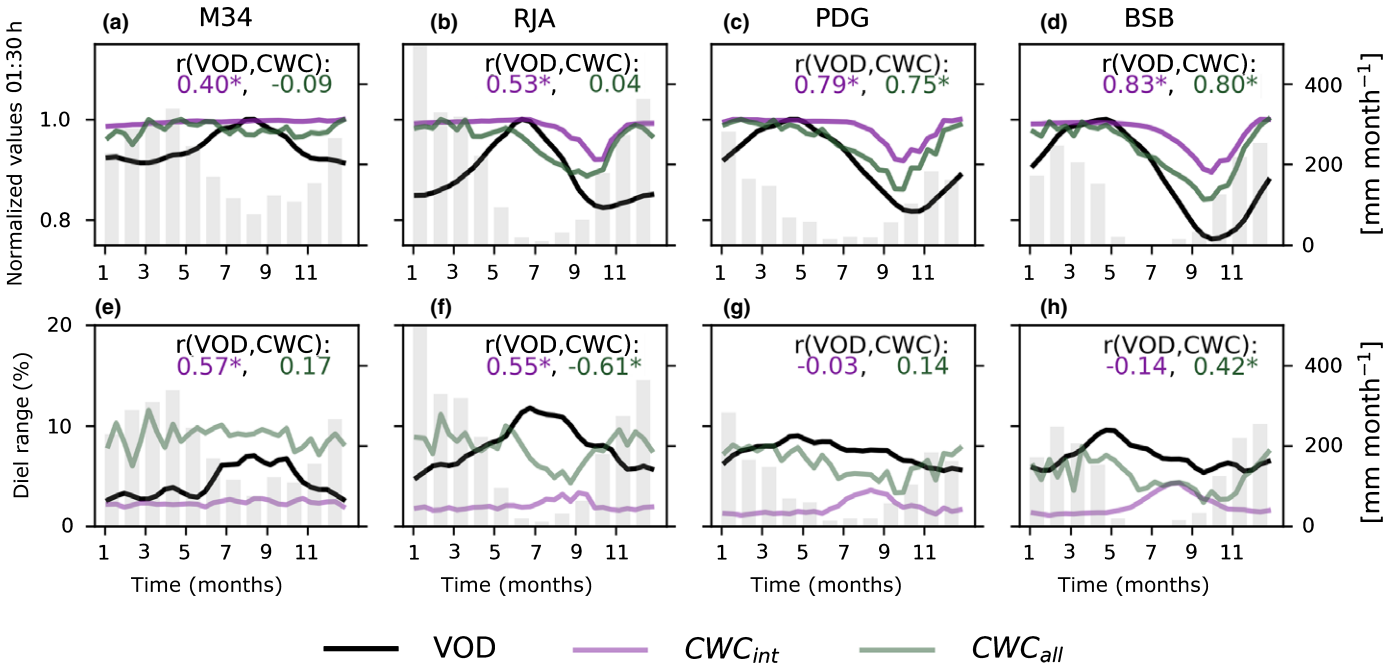

Fig. 6 Comparison of average seasonality between vegetation optical depth (VOD) and simulated canopy water content (CWC) across four study sites. (a–d) seasonality of 01:30 h VOD (black), CWC_{all} (including leaf surface water, green), and CWC_{int} (excluding leaf surface water, purple). To facilitate comparison, we normalized the seasonality by dividing by the maximum seasonal values for each variable. (e–h) similar to (a–d) but for diurnal ranges, calculated as $(1 - X_{13:30\ h}/X_{01:30\ h}) \times 100\%$, where X denotes either VOD or CWC. We calculated Pearson's r between the average seasonality in VOD and the simulated CWC (with and without leaf surface water) and showed the correlation coefficients using the same color as the different CWC lines. Significant correlations ($P < 0.05$) are marked with an asterisk (*). In all plots, we only included water from the top 1 kgC m^{-2} biomass within the canopy, and gray bars represent average monthly rainfall. M34, Manaus K34 site; RJA, Reserva Jaru site; PDG, Pé-de-Gigante; BSB, Brasília site.

At the inter-annual timescale, VOD showed substantial variability relative to its average seasonality in both 01:30 h values and diurnal ranges (Fig. 7) due to changes in hydroclimatic conditions. Simulated anomalies in both CWC_{all} and CWC_{int} at 01:30 h were more strongly correlated with anomalies in 01:30 h VOD at the drier sites (significant positive correlation with Pearson's r values ranging from 0.36 to 0.53 for PDG and BSB) than at the wet sites (no significant correlations). While including LW_s increased the correlation coefficients by 0.05 to 0.2, it did not change the general cross-site pattern. The simulated diurnal range anomalies in CWC were not correlated with the diurnal range anomalies in VOD at inter-annual time scales, regardless of whether or not LW_s was included (Fig. 7e–h). The simulated diurnal range in CWC generally showed less inter-annual variability, with standard deviations of 1.0–1.7% for CWC_{all} and 0.19–0.37% for CWC_{int}, than the diurnal range in VOD, which had standard deviations ranging from 1.9% to 2.2%. Similar to the seasonal-scale analysis, correcting for WW_i did not change the simulated patterns of inter-annual variations in CWC (Fig. S10).

Discussion

Predicted CWC and its relationship with VOD

The increasing use of VOD to infer large-scale patterns of vegetation water stress builds on the mechanistic proportionality between VOD and CWC (Konings *et al.*, 2019). However, quantitative assessments of this relationship have been lacking at the ecosystem scale – the scale at which remote sensing VOD measurements are made (tens of km) – particularly in humid, high-biomass ecosystems such as tropical forests. This is mostly because ground-based measurements of CWC are generally made at the level of leaves or tree branches (Powers & Tiffin, 2010; Chavana-Bryant *et al.*, 2016; Martin *et al.*, 2018). Consequently, previous VOD field evaluation studies (Liu *et al.*, 2015; Chaparro *et al.*, 2019; Fan *et al.*, 2019) only examined the statistical associations between spatial variation in VOD and above-ground biomass, a quantity that is easier to measure at larger spatial scales via forest inventory and LiDAR measurements.

Our study evaluates, for the first time, the VOD–CWC relationship in both the spatial and temporal domains through novel application of a terrestrial biosphere model. Our analyses support our first hypothesis (H1), that VOD scales approximately linearly with CWC across space and time; however, it also reveals important sources of complexity in this relationship: the slope of the VOD–CWC relationship varied across sites with different moisture conditions and vegetation structures (Fig. 4). While some variation in the slope with vegetation type is expected, a threefold increase in the slope from savanna to forest sites (Fig. 4d) is far greater than previously estimated from radiometric experiments in nonforested ecosystems (Van De Griend & Wigneron, 2004) and leads to a relatively sigmoidal or saturating VOD–CWC relationship for cross-site variations.

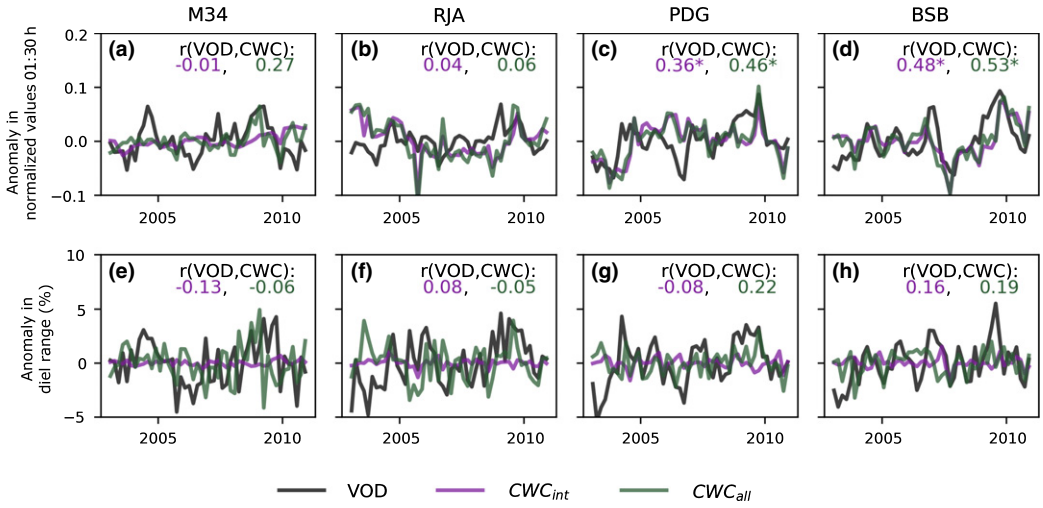

Fig. 7 Comparison of inter-annual variability between vegetation optical depth (VOD) and simulated canopy water content (CWC) after removing average seasonality across the four study sites. (a–d) variability of 01:30 h VOD (black), CWC_{all} (including leaf surface water, green), and CWC_{int} (excluding leaf surface water, purple). We normalized the time series by dividing by the maximum as in Fig. 6. (e–h) similar to (a–d) but for diurnal ranges calculated as $(1 - X_{13:30\ h}/X_{01:30\ h}) \times 100\%$, where X denotes either VOD or CWC. We calculated Pearson's r between the average seasonality in VOD and the simulated CWC (with and without leaf surface water) and showed the correlation coefficients using the same color as the different CWC lines. Significant correlations ($P < 0.05$) were marked with an asterisk (*). In all plots, we only included water from the top 1 kgC m^{-2} biomass. Due to high-frequency variation in the simulated CWC, we averaged the biweekly data into bimonthly values to facilitate comparison. M34, Manaus K34 site; RJA, Reserva Jaru site; PDG, Pé-de-Gigante; BSB, Brasília site.

Vegetation optical depth saturation at high aboveground biomass density (Chaparro *et al.*, 2019) should not be the primary factor driving variation in the VOD–CWC slopes because cross-site variation in penetration depth is explicitly considered in our analysis (Fig. S3), although our approach might not fully capture small seasonal changes of penetration depth within each site. The larger-than-expected variation in the VOD–CWC slope may reflect deficiencies in the model formulation: most notably, the model's drought-driven phenology scheme generated smaller-than-observed seasonal amplitudes in CWC at the two wet sites, compared to the seasonality in VOD (Fig. 6), which may explain the low R^2 and slope values for M34 and RJA. The cross-site variation in the slope values for the VOD–CWC relationship could also be due to uncertainty in the VOD retrievals, particularly the uncertainty associated with surface temperature and single-scattering albedo in the densely forested M34 and RJA sites (Du *et al.*, 2017) or due to multiple scattering (Schwank *et al.*, 2018). Both explanations call for additional calibration of VOD with *in-situ* measurements of CWC, especially in moist, high-humidity ecosystems such as tropical forests.

The role of LW_s in CWC and VOD variation across different time scales

Our simulations explicitly consider dew formation, rainfall interception, and the resulting dynamics of LW_s. While no direct measurements of canopy LW_s temporal dynamics are available to evaluate the model's predictions, the simulated range of LW_s is consistent with sparse sampling from an Amazonian moist forest (Fig. S2). In addition, a rare ground-based radiometer study in a Panamanian tropical moist forest (Schneebeli *et al.*, 2011) estimated that whole-canopy LW_s could regularly reach 0.17 $kgH_2O\ m^{-2}$ (ground) at pre-dawn from dew formation, and intensive rainfall events occasionally increased LW_s to 0.4–1 $kgH_2O\ m^{-2}$. The model generated comparable average predawn LW_s values of 0.21–0.23 $kgH_2O\ m^{-2}$ for the two tropical forest sites (Fig. S6). The simulated average predawn LW_s is close to the observed dew-driven value but lower than the observed rainfall-driven values, likely because reanalysis rainfall underestimates the diurnal cycle (Fig. S11).

In our model simulations, LW_s accounts for > 50% of diurnal variation in CWC at all four of the study sites (Fig. 3). The large diurnal contribution from the relatively small LW_s pool (< 10% of total CWC) stems from its fast turnover rate: by midday almost all LW_s accumulated during the night evaporates away (Fig. 3). By contrast, simulated LW_i varied by only 10–15% within a day, and WW_i by even less. In nature and in the model, this occurs because plant stomatal control constrains daily minimum leaf water potential to be above, or not far below, the leaf turgor loss point (Brodribb & Holbrook, 2003; Fontes *et al.*, 2018), which corresponds to a relative water content value of *c.* 90% for tropical wet forests (Bartlett *et al.*, 2012).

Consequently, our results call into question the ability to correctly infer spatial and temporal patterns of plant water stress from diurnal measurements of VOD in humid forest ecosystems such as tropical rainforests, as illustrated in our isohydricity analysis (Fig. 5). First, LW_s dynamics might contribute most to the VOD-based isohydricity. Second, isohydricity index based on water content is influenced by both LW_i stress and the seasonal variation in vegetation structure, and thus can deviate from the isohydricity index based on leaf water potential and converge to 1 (Fig. 5i–p). In addition, if VOD diurnal range reflects diurnal

water stress, it should peak in the dry season in tropical forests – when plant diurnal water stress is generally the highest – as shown in the observations of Brodribb & Holbrook (2004) and Fisher *et al.* (2006) and the biosphere model simulations conducted in this study (Fig. 2). However, at the two savanna sites, VOD diurnal range peaked in late wet season, which can only be explained by including LW_s (Fig. 6). The exclusion of rainy days (Konings & Gentine, 2017; Li *et al.,* 2017) is likely not enough to eliminate the effects of LW_s on CWC because dew formation can also significantly contribute to LW_s and the simulated importance of LW_s only drops to a low level in months with both low rainfall and humidity (Fig. S12). Hence, the influence of LW_s on VOD retrievals may also be important in other humid ecosystems, such as those found along the North American Pacific coast (Burgess & Dawson, 2004) and montane forests (Berry *et al.,* 2014).

The importance of LW_s decreases, however, at the seasonal and inter-annual time scales (Figs 6, 7), implying that failing to consider LW_s will have less of an effect on VOD-based inference of canopy phenology (Guan *et al.,* 2014; Wang *et al.,* 2020) and vegetation mortality (Rao *et al.,* 2019; Wigneron *et al.,* 2020). Therefore, our results support our second hypothesis (H2), that the contribution of LW_s is highest at the diurnal time scale.

By contrast, there is only partial support for our third hypothesis (H3), that the contribution of LW_s to diurnal VOD dynamics increases as precipitation increases: variance decomposition implies that an increasing contribution from LW_s along the gradient from dry to wet sites (Fig. 3) and from wet to dry months (Fig. S12) is consistent with H3. However, it is difficult to draw strong conclusions regarding H3 given the large uncertainties in VOD retrievals and low level of seasonality in the model simulations compared to the observed seasonality of VOD values and diurnal ranges at the two moist forest sites (Fig. 6). In addition, the simulated cross-site variations in the LW_s contribution might be biased because ED-2.2-hydro does not represent possible leaf trait adaptation across moisture gradients, such as changes in leaf texture and trichome abundance, that could regulate LW_s retention (Aparecido *et al.,* 2017) and thus influence LW_s dynamics. Further *in situ* data collection and model improvement and benchmarking are necessary to accurately evaluate how the LW_s contribution varies across moisture gradients.

Implications for tropical phenology in vegetation models

Our model-data analysis also provides a useful evaluation of the plant hydrodynamics and leaf phenology formulations in the ED-2.2-hydro terrestrial biosphere model. As anticipated, there was better agreement between the model predictions and the VOD measurements at the two drier sites, where abiotic moisture conditions exhibit large variability that significantly affects CWC. However, the predicted seasonal decline of LAI is later than in MODIS LAI estimates (Fig. 1), and the relative magnitude of the seasonal decline in CWC was smaller than in the VOD observations (Fig. 6), suggesting that the model's drought-deciduous leaf phenology scheme may not be sufficiently responsive to seasonal water stress. In the current model formulation, leaf-drop is triggered when pre-dawn water potential falls below the turgor loss point, whereas drought experiments on tropical seedlings suggest that the average of pre-dawn and midday water potential can best predict leaf shedding (Wolfe *et al.,* 2016). Incorporating midday water potential into the drought-deciduous phenology scheme might therefore improve the seasonality at drier savanna sites.

Similarly, at the two wet sites, the predicted seasonality in CWC was lower than the seasonality in VOD (Fig. 6). This may be because the VOD seasonality is partially attributable to unknown retrieval errors caused by seasonally varying properties (e.g. changes in canopy structure) in densely vegetated areas (Konings *et al.,* 2016; Du *et al.,* 2017). Another possible explanation is that biotic factors such as leaf ontogeny can influence seasonal variation in CWC under moist conditions. For instance, leaf relative water content can change substantially with leaf age in tropical wet forests (Chavana-Bryant *et al.,* 2016); seasonal changes in leaf demography at tropical moist forests (Wu *et al.,* 2016) may therefore contribute to seasonal variation in CWC and resulting VOD measurements. A simple calculation of CWC changes based on published leaf demography and leaf ontogeny data at Manaus (Chavana-Bryant *et al.,* 2016; Wu *et al.,* 2016) suggests that seasonal variation in leaf age could explain the seasonal amplitude of VOD at M34, albeit with a 1–2 month lag in timing (Fig. S13).

Conclusions

Our analyses indicate that LW_s makes a large contribution to diurnal variation in landscape-scale CWC and AMSR-E VOD signals over tropical forests. This is important because diurnal variation in VOD has been proposed as a measure of canopy isohydricity, a metric widely used to diagnose the water status of plant canopies. Our analysis shows that LW_s also influences seasonal variation in VOD, but to a far lesser extent. In this analysis, we examined VOD measurements from X-band microwave instruments that have relatively low penetration into the dense canopies of tropical forests; however, our findings also apply to VOD measurements from lower (L-band) electromagnetic frequencies (e.g. the Soil Moisture Active Passive (SMAP) and Soil Moisture and Ocean Salinity (SMOS) satellites) because the simulated LW_s contributions remained high even when we evaluated greater canopy penetration depth (Fig. S6). Future applications of microwave band measurements, as well as other imaging and spectroscopy-based estimates of CWC (Asner *et al.,* 2016) should therefore carefully consider the effects of variation in LW_s, particularly during rainy and humid periods. In turn, the sensitivity of VOD to LW_s newly identified in this study provides new opportunities to understand LW_s dynamics and their impact on plant water use.

Our analyses also highlight the value of explicitly representing plant hydrodynamics in terrestrial biosphere model formulations. The consistency between VOD and model predicted CWC across diurnal, seasonal, and inter-annual timescales at the two tropical savanna sites suggests that the current model structure is able to capture important processes governing plant hydrodynamics; however, capturing diurnal and seasonal patterns of

VOD in wet tropical forests is likely to require consideration of phenological processes affecting CWC, such as seasonal leaf demography and ontogeny.

Acknowledgements

This research was supported by NASA Earth Sciences grant (16-CARBON16-0130) to PM, SS and AK. The research carried out at the Jet Propulsion Laboratory, California Institute of Technology, was under a contract with the National Aeronautics and Space Administration. ML was supported by the NASA Postdoctoral Program, administered by Universities Space Research Association under contract with NASA. The authors thank O. Binks for sharing leaf surface water data in an Amazon moist forest and constructive comments from K. Caylor and two anonymous reviewers.

Author contributions

XX, PM, AK and SS designed the research. ML and XX processed the meteorology and flux tower data. AK and AF processed AMSR-E VOD data. LX and SS provided GLAS LiDAR LAI data. DW provided the MODIS data. JW provided the *in-situ* leaf trait and demography data. XX performed model simulation, conducted analyses, and drafted the manuscript. All authors contributed to the writing of the manuscript.

ORCID

Andrew Feldman https://orcid.org/0000-0003-1547-6995
Alexandra G. Konings https://orcid.org/0000-0002-2810-1722
Marcos Longo https://orcid.org/0000-0001-5062-6245
Paul Moorcroft https://orcid.org/0000-0002-2876-4673
Sassan Saatchi https://orcid.org/0000-0001-8524-4917
Donghai Wu https://orcid.org/0000-0002-4638-3743
Jin Wu https://orcid.org/0000-0001-8991-3970
Liang Xu https://orcid.org/0000-0001-7400-3827
Xiangtao Xu https://orcid.org/0000-0002-9402-9474

Data availability

The remote sensing data that support the findings of this study are openly available at http://files.ntsg.umt.edu/data/LPDR_v2/ for VOD, https://nsidc.org/data/icesat/data.html for GLAS, and https://lpdaac.usgs.gov/ for MODIS. The ED2 model codes are archived at https://doi.org/10.5281/zenodo.3978588. The meteorological forcing data used to drive ED2 are available from the corresponding author upon request.

References

Anderegg WRL, Konings AG, Trugman AT, Yu K, Bowling DR, Gabbitas R, Karp DS, Pacala S, Sperry JS, Sulman BN *et al.* 2018. Hydraulic diversity of forests regulates ecosystem resilience during drought. *Nature* **561**: 538–541.

Aparecido LMT, Miller GR, Cahill AT, Moore GW. 2017. Leaf surface traits and water storage retention affect photosynthetic responses to leaf surface wetness among wet tropical forest and semiarid savanna plants. *Tree Physiology* **37**: 1285–1300.

Asner GP, Brodrick PG, Anderson CB, Vaughn N, Knapp DE, Martin RE. 2016. Progressive forest canopy water loss during the 2012–2015 California drought. *Proceedings of the National Academy of Sciences, USA* **113**: E249–E255.

Bartlett MK, Scoffoni C, Sack L. 2012. The determinants of leaf turgor loss point and prediction of drought tolerance of species and biomes: a global meta-analysis. *Ecology Letters* **15**: 393–405.

Beck HE, Wood EF, Pan M, Fisher CK, Miralles DG, Van Dijk AIJM, McVicar TR, Adler RF. 2019. MSWep v2 Global 3-hourly 0.1° precipitation: methodology and quantitative assessment. *Bulletin of the American Meteorological Society* **100**: 473–500.

Berry ZC, White JC, Smith WK. 2014. Foliar uptake, carbon fluxes and water status are affected by the timing of daily fog in saplings from a threatened cloud forest. *Journal of Refugee Studies* **34**: 459–470.

Binks O, Finnigan J, Coughlin I, Disney M, Calders K, Burt A, Vicari MB, da Costa AL, Mencuccini M, Meir P. 2021. Canopy wetness in the Eastern Amazon. *Agricultural and Forest Meteorology* **297**: 108250.

Binks O, Mencuccini M, Rowland L, da Costa ACL, de Carvalho CJR, Bittencourt P, Eller C, Teodoro GS, Carvalho EJM, Soza A *et al.* 2019. Foliar water uptake in Amazonian trees: Evidence and consequences. *Global Change Biology* **25**: 2678–2690.

Brodribb TJ, Holbrook NM. 2003. Stomatal closure during leaf dehydration, correlation with other leaf physiological traits. *Plant Physiology* **132**: 2166–2173.

Brodribb TJ, Holbrook NM. 2004. Diurnal depression of leaf hydraulic conductance in a tropical tree species. *Plant, Cell & Environment* **27**: 820–827.

Bucci SJ, Goldstein G, Meinzer FC, Franco AC, Campanello P, Scholz FG. 2005. Mechanisms contributing to seasonal homeostasis of minimum leaf water potential and predawn disequilibrium between soil and plant water potential in Neotropical savanna trees. *Trees - Structure and Function* **19**: 296–304.

Burgess SSO, Dawson TE. 2004. The contribution of fog to the water relations of *Sequoia sempervirens* (D. Don): foliar uptake and prevention of dehydration. *Plant, Cell & Environment* **27**: 1023–1034.

Calvet JC, Wigneron JP, Mougin E, Kerr YH, Brito JLS. 1994. Plant water content and temperature of the Amazon forest from satellite microwave radiometry. *IEEE Transactions on Geoscience and Remote Sensing* **32**: 397–408.

Chaparro D, Duveiller G, Piles M, Cescatti A, Vall-llossera M, Camps A, Entekhabi D. 2019. Sensitivity of L-band vegetation optical depth to carbon stocks in tropical forests: a comparison to higher frequencies and optical indices. *Remote Sensing of Environment* **232**: 111303.

Chavana-Bryant C, Malhi Y, Wu J, Asner GP, Anastasiou A, Enquist BJ, Cosio Caravasi EG, Doughty CE, Saleska SR, Martin RE *et al.* 2016. Leaf aging of Amazonian canopy trees as revealed by spectral and physiochemical measurements. *New Phytologist* **214**: 1049–1063.

Christoffersen BO, Gloor M, Fauset S, Fyllas NM, Galbraith DR, Baker TR, Kruijt B, Rowland L, Fisher RA, Binks OJ *et al.* 2016. Linking hydraulic traits to tropical forest function in a size-structured and trait-driven model (TFS v.1-Hydro). *Geoscientific Model Development* **9**: 4227–4255.

Cosh MH, Tao J, Jackson TJ, McKee L, O'Neil PE. 2010. Vegetation water content mapping in a diverse agricultural landscape: National Airborne Field Experiment 2006. *Journal of Applied Remote Sensing* **4**: 43532.

De Kauwe MG, Medlyn BE, Ukkola AM, Mu M, Sabot MEB, Pitman AJ, Meir P, Cernusak LA, Rifai SW, Choat B *et al.* 2020. Identifying areas at risk of drought-induced tree mortality across South-Eastern Australia. *Global Change Biology* **26**: 5716–5733.

Didan K. 2015. *MOD13A1 MODIS/Terra vegetation indices 16-Day L3 global 500m SIN grid V006.* NASA EOSDIS Land Processes DAAC 10. [WWW document] URL https://ladsweb.modaps.eosdis.nasa.gov/missions-and-measurements/products/MOD13A1/.

Du J, Jackson TJ, Bindlish R, Cosh MH, Li L, Hornbuckle BK, Kabela ED. 2012. Effect of dew on aircraft-based passive microwave observations over an agricultural domain. *Journal of Applied Remote Sensing* **6**: 63571–63581.

Du J, Kimball JS, Jones LA, Kim Y, Glassy J, Watts JD. 2017. A global satellite environmental data record derived from AMSR-E and AMSR2 microwave Earth observations. *Earth System Science Data* **9**: 791–808.

Eller CB, Lima AL, Oliveira RS. 2013. Foliar uptake of fog water and transport belowground alleviates drought effects in the cloud forest tree species, *Drimys brasiliensis* (Winteraceae). *New Phytologist* **199**: 151–162.

Fan L, Wigneron JP, Ciais P, Chave J, Brandt M, Fensholt R, Saatchi SS, Bastos A, Al-Yaari A, Hufkens K *et al.* 2019. Satellite-observed pantropical carbon dynamics. *Nature Plants* **5**: 944–951.

Fatichi S, Pappas C, Ivanov VY. 2016. Modeling plant–water interactions: an ecohydrological overview from the cell to the global scale. *Wiley Interdisciplinary Reviews: Water* **3**: 327–368.

Feldman AF, Short Gianotti DJ, Trigo IF, Salvucci GD, Entekhabi D. 2020. Land–atmosphere drivers of landscape-scale plant water content loss. *Geophysical Research Letters* **47**: e2020GL090331.

Fisher RA, Williams M, Do Vale RL, Da Costa AL, Meir P. 2006. Evidence from Amazonian forests is consistent with isohydric control of leaf water potential. *Plant, Cell & Environment* **29**: 151–165.

Fontes CG, Dawson TE, Jardine K, McDowell N, Gimenez BO, Anderegg L, Negrón-Juárez R, Higuchi N, Fine PVA, Araújo AC *et al.* 2018. Dry and hot: the hydraulic consequences of a climate change-type drought for Amazonian trees. *Philosophical Transactions of the Royal Society of London. Series B: Biological Sciences* **373**: 20180209.

Funk C, Peterson P, Landsfeld M, Pedreros D, Verdin J, Shukla S, Husak G, Rowland J, Harrison L, Hoell A *et al.* 2015. The climate hazards infrared precipitation with stations – a new environmental record for monitoring extremes. *Scientific Data* **2**: 1–21.

Gelaro R, McCarty W, Suárez MJ, Todling R, Molod A, Takacs L, Randles CA, Darmenov A, Bosilovich MG, Reichle R *et al.* 2017. The modern-era retrospective analysis for research and applications, version 2 (MERRA-2). *Journal of Climate* **30**: 5419–5454.

Gerlein-Safdi C, Gauthier PPG, Caylor KK. 2018a. Dew-induced transpiration suppression impacts the water and isotope balances of *Colocasia* leaves. *Oecologia* **187**: 1041–1051.

Gerlein-Safdi C, Koohafkan MC, Chung M, Rockwell FE, Thompson S, Caylor KK. 2018b. Dew deposition suppresses transpiration and carbon uptake in leaves. *Agricultural and Forest Meteorology* **259**: 305–316.

de Gonçalves LGG, Restrepo-Coupe N, da Rocha HR, Saleska SR, Stockli R. 2013. *LBA-ECO CD-32 LBA Model Intercomparison Project (LBA-MIP) Forcing Data*. Oak Ridge, TN, USA: ORNL DAAC.

Grossiord C, Sevanto S, Borrego I, Chan AM, Collins AD, Dickman LT, Hudson PJ, McBranch N, Michaletz ST, Pockman WT *et al.* 2017. Tree water dynamics in a drying and warming world. *Plant, Cell & Environment* **40**: 1861–1873.

Guan K, Wood EF, Medvigy D, Kimball J, Pan M, Caylor KK, Sheffield J, Xu X, Jones MO. 2014. Terrestrial hydrological controls on land surface phenology of African savannas and woodlands. *Journal of Geophysical Research: Biogeosciences* **119**: 1652–1669.

Guglielmetti M, Schwank M, Mätzler C, Oberdörster C, Vanderborght J, Flühler H. 2007. Measured microwave radiative transfer properties of a deciduous forest canopy. *Remote Sensing of Environment* **109**: 523–532.

INPE. 2020. *SONDA - Sistema de Organização Nacional de Dados Ambientais*. Instituto Nacional de Pesquisas Espaciais. [WWW document] URL http://sonda.ccst.inpe.br/ [accessed 29 January 2021].

Jackson TJ, Schmugge TJ. 1991. Vegetation effects on the microwave emission of soils. *Remote Sensing of Environment* **36**: 203–212.

Jones LA, Kimball JS, Zhang K, Jones LA, Kimball JS, Zhang K, Ferguson CR, Wood EF, Chan STK, Njoku EG *et al.* 2010. Satellite microwave remote sensing of daily land surface air temperature minima and maxima from AMSR-E. *IEEE Journal of Selected Topics in Applied Earth Observations and Remote Sensing* **3**: 111–123.

Jones LA, Kimball JS. 2012. Daily global land surface parameters derived from AMSR-E, Version 1.

Junqueira Junior JA, de Mello CR, de Mello JM, Scolforo HF, Beskow S, McCarter J. 2019. Rainfall partitioning measurement and rainfall interception modelling in a tropical semi-deciduous Atlantic forest remnant. *Agricultural and Forest Meteorology* **275**: 170–183.

Kennedy D, Swenson S, Oleson KW, Lawrence DM, Fisher R, Lola da Costa AC, Gentine P. 2019. Implementing plant hydraulics in the community land model, version 5. *Journal of Advances in Modeling Earth Systems* **11**: 485–513.

Konings AG, Gentine P. 2017. Global variations in ecosystem-scale isohydricity. *Global Change Biology* **23**: 891–905.

Konings AG, Piles M, Rötzer K, McColl KA, Chan SK, Entekhabi D. 2016. Vegetation optical depth and scattering albedo retrieval using time series of dual-polarized L-band radiometer observations. *Remote Sensing of Environment* **172**: 178–189.

Konings AG, Rao K, Steele-Dunne SC. 2019. Macro to micro: microwave remote sensing of plant water content for physiology and ecology. *New Phytologist* **223**: 1166–1172.

Lakatos M, Obregón A, Büdel B, Bendix J. 2012. Midday dew – an overlooked factor enhancing photosynthetic activity of corticolous epiphytes in a wet tropical rain forest. *New Phytologist* **194**: 245–253.

Li Y, Guan K, Gentine P, Konings AG, Meinzer FC, Kimball JS, Xu X, Anderegg WRL, McDowell NG, Martinez-Vilalta J *et al.* 2017. Estimating global ecosystem isohydry/anisohydry using active and passive microwave satellite data. *Journal of Geophysical Research: Biogeosciences* **122**: 3306–3321.

Liu YY, Van Dijk AIJM, De Jeu RAM, Canadell JG, McCabe MF, Evans JP, Wang G. 2015. Recent reversal in loss of global terrestrial biomass. *Nature Climate Change* **5**: 470–474.

Longo M. 2014. *Amazon forest response to changes in rainfall regime: Results from an individual-based dynamic vegetation model*. Ph.D. Thesis, Harvard University. [WWW document] URL https://ui.adsabs.harvard.edu/abs/2014PhDT.....5L [accessed 14 February 2021].

Longo M, Knox RG, Medvigy DM, Levine NM, Dietze MC, Kim Y, Swann ALS, Zhang K, Rollinson CR, Bras RL *et al.* 2019. The biophysics, ecology, and biogeochemistry of functionally diverse, vertically and horizontally heterogeneous ecosystems: The Ecosystem Demography model, version 2.2-Part 1: Model description. *Geoscientific Model Development* **12**: 4309–4346.

MacArthur RH, Horn HS. 1969. Foliage profile by vertical measurements. *Ecology* **50**: 802–804.

Macelloni G, Paloscia S, Pampaloni P, Ruisi R. 2001. Airborne multifrequency L- to Ka- band radiometric measurements over forests. *IEEE Transactions on Geoscience and Remote Sensing* **39**: 2507–2513.

Martin RE, Asner GP, Francis E, Ambrose A, Baxter W, Das AJ, Vaughn NR, Paz-Kagan T, Dawson T, Nydick K *et al.* 2018. Remote measurement of canopy water content in giant sequoias (*Sequoiadendron giganteum*) during drought. *Forest Ecology and Management* **419–420**: 279–290.

Martínez-Vilalta J, Poyatos R, Aguadé D, Retana J, Mencuccini M. 2014. A new look at water transport regulation in plants. *New Phytologist* **204**: 105–115.

McDowell NG, Michaletz ST, Bennett KE, Solander KC, Xu C, Maxwell RM, Middleton RS. 2018. Predicting chronic climate-driven disturbances and their mitigation. *Trends in Ecology and Evolution* **33**: 15–27.

Medvigy D, Wofsy SC, Munger JW, Hollinger DY, Moorcroft PR. 2009. Mechanistic scaling of ecosystem function and dynamics in space and time: Ecosystem Demography model version 2. *Journal of Geophysical Research: Biogeosciences* **114**: G01002.

Mencuccini M, Manzoni S, Christoffersen B. 2019. Modelling water fluxes in plants: from tissues to biosphere. *New Phytologist* **222**: 1207–1222.

Momen M, Wood JD, Novick KA, Pangle R, Pockman WT, McDowell NG, Konings AG. 2017. Interacting effects of leaf water potential and biomass on vegetation optical depth. *Journal of Geophysical Research: Biogeosciences* **122**: 3031–3046.

Ni-Meister W, Jupp DLB, Dubayah R. 2001. Modeling lidar waveforms in heterogeneous and discrete canopies. *IEEE Transactions on Geoscience and Remote Sensing* **39**: 1943–1958.

Novick KA, Ficklin DL, Stoy PC, Williams CA, Bohrer G, Oishi AC, Papuga SA, Blanken PD, Noormets A, Sulman BN *et al.* 2016. The increasing importance of atmospheric demand for ecosystem water and carbon fluxes. *Nature Climate Change* **6**: 1023–1027.

Powell TL, Koven CD, Johnson DJ, Faybishenko B, Fisher RA, Knox RG, McDowell NG, Condit R, Hubbell SP, Wright SJ *et al.* 2018. Variation in hydroclimate sustains tropical forest biomass and promotes functional diversity. *New Phytologist* **219**: 932–946.

Powell TL, Wheeler JK, de Oliveira AAR, da Costa ACL, Saleska SR, Meir P, Moorcroft PR. 2017. Differences in xylem and leaf hydraulic traits explain

differences in drought tolerance among mature Amazon rainforest trees. *Global Change Biology* **23**: 4280–4293.

Powers JS, Tiffin P. 2010. Plant functional type classifications in tropical dry forests in Costa Rica: leaf habit versus taxonomic approaches. *Functional Ecology* **24**: 927–936.

Rao K, Anderegg WRL, Sala A, Martínez-Vilalta J, Konings AG. 2019. Satellite-based vegetation optical depth as an indicator of drought-driven tree mortality. *Remote Sensing of Environment* **227**: 125–136.

Restrepo-Coupe N, Levine NM, Christoffersen BO, Albert LP, Wu J, Costa MH, Galbraith D, Imbuzeiro H, Martins G, da Araujo AC *et al.* 2017. Do dynamic global vegetation models capture the seasonality of carbon fluxes in the Amazon basin? A data–model intercomparison. *Global Change Biology* **23**: 191–208.

Schimel D, Schneider FD. 2019. Flux towers in the sky: global ecology from space. *New Phytologist* **224**: 570–584.

Schneebeli M, Wolf S, Kunert N, Eugster W, Mätzler C. 2011. Relating the X-band opacity of a tropical tree canopy to sapflow, rain interception and dew formation. *Remote Sensing of Environment* **115**: 2116–2125.

Schwank M, Naderpour R, Mätzler C. 2018. 'Tau-Omega'- and Two-Stream emission models used for passive L-Band retrievals: application to close-range measurements over a forest. *Remote Sensing* **10**: 1868.

Tang H, Dubayah R, Brolly M, Ganguly S, Zhang G. 2014. Large-scale retrieval of leaf area index and vertical foliage profile from the spaceborne waveform lidar (GLAS/ICESat). *Remote Sensing of Environment* **154**: 8–18.

Tang H, Dubayah R. 2017. Light-driven growth in Amazon evergreen forests explained by seasonal variations of vertical canopy structure. *Proceedings of the National Academy of Sciences, USA* **114**: 2640–2644.

Tian F, Brandt M, Liu YY, Verger A, Tagesson T, Diouf AA, Rasmussen K, Mbow C, Wang Y, Fensholt R. 2016. Remote sensing of vegetation dynamics in drylands: evaluating vegetation optical depth (VOD) using AVHRR NDVI and *in situ* green biomass data over West African Sahel. *Remote Sensing of Environment* **177**: 265–276.

Van De Griend AA, Wigneron JP. 2004. On the measurement of microwave vegetation properties: some guidelines for a protocol. *IEEE Transactions on Geoscience and Remote Sensing* **42**: 2277–2289.

Wang X, Dannenberg MP, Yan D, Jones MO, Kimball JS, Moore DJP, van Leeuwen WJD, Didan K, Smith WK. 2020. Globally consistent patterns of asynchrony in vegetation phenology derived from optical, microwave, and fluorescence satellite data. *Journal of Geophysical Research Biogeosciences* **125**: e2020JG005732.

Wigneron JP, Fan L, Ciais P, Bastos A, Brandt M, Chave J, Saatchi S, Baccini A, Fensholt R. 2020. Tropical forests did not recover from the strong 2015–2016 El Niño event. *Science Advances* **6**: eaay4603.

Wigneron JP, Jackson TJ, O'Neill P, De Lannoy G, de Rosnay P, Walker JP, Ferrazzoli P, Mironov V, Bircher S, Grant JP *et al.* 2017. Modelling the passive microwave signature from land surfaces: a review of recent results and application to the L-band SMOS & SMAP soil moisture retrieval algorithms. *Remote Sensing of Environment* **192**: 238–262.

Wolfe BT, Sperry JS, Kursar TA. 2016. Does leaf shedding protect stems from cavitation during seasonal droughts? A test of the hydraulic fuse hypothesis. *New Phytologist* **212**: 1007–1018.

Wu J, Albert LP, Lopes AP, Restrepo-Coupe N, Hayek M, Wiedemann KT, Guan K, Stark SC, Christoffersen B, Prohaska N *et al.* 2016. Leaf development and demography explain photosynthetic seasonality in Amazon evergreen forests. *Science* **351**: 972–976.

Wu J, Serbin SP, Ely KS, Wolfe BT, Dickman LT, Grossiord C, Michaletz ST, Collins AD, Detto M, McDowell NG *et al.* 2020. The response of stomatal conductance to seasonal drought in tropical forests. *Global Change Biology* **26**: 823–839.

Xu X, Medvigy D, Powers JS, Becknell JM, Guan K. 2016. Diversity in plant hydraulic traits explains seasonal and inter-annual variations of vegetation dynamics in seasonally dry tropical forests. *New Phytologist* **212**: 80–95.

Yang Y, Saatchi SS, Xu L, Yu Y, Choi S, Phillips N, Kennedy R, Keller M, Knyazikhin Y, Myneni RB. 2018. Post-drought decline of the Amazon carbon sink. *Nature Communications* **9**: 3172.

Zhang Y, Zhou S, Gentine P, Xiao X. 2019. Can vegetation optical depth reflect changes in leaf water potential during soil moisture dry-down events? *Remote Sensing of Environment* **234**: 111451.

Zwally HJ, Schutz R, Hancock D, Dimarzio J. 2014. GLAS/ICESat L2 Global Land Surface Altimetry Data (HDF5), Version 34. NASA National Snow and Ice Data Center Distributed Active Archive Center, doi: 10.5067/ICESAT/GLAS/DATA211

Supporting Information

Additional Supporting Information may be found online in the Supporting Information section at the end of the article.

Fig. S1 Average monthly seasonality of the meteorological forcing used to drive the model simulations.

Fig. S2 Distribution of predawn leaf surface water (LW_s) in the canopy top compared with observed ranges.

Fig. S3 Schematic diagram of penetration depth for canopy water content (CWC) in the hydrodynamics-enabled version of Ecosystem Demography v.2.2 (ED-2.2-hydro).

Fig. S4 Vertical profile and average seasonality of simulated wood water potential at the base of tree stems.

Fig. S5 Average seasonality of evapotranspiration from ED-2.2-hydro simulations (red line) and flux tower data.

Fig. S6 Contribution of LW_s to CWC in model simulations using 10 kgC m^{-2} as penetration depth.

Fig. S7 Relationship between VOD and simulated CWC_{all} (including LW_s) and CWC_{int} (excluding LW_s) using 10 kgC m^{-2} as penetration depth.

Fig. S8 Average seasonality of simulated LW_s.

Fig. S9 Average seasonality of VOD and CWC corrected by leaf water potential.

Fig. S10 Deseasoned multi-year variability of VOD and CWC corrected by leaf water potential.

Fig. S11 Average diurnal cycles of precipitation rainfall from ground-observation (GRND) and reanalysis data (REAN) used in our simulations.

Fig. S12 Relative contribution of variance in LW_s to the diurnal variance in CWC_{all} as a function of precipitation and vapor pressure deficit.

Fig. S13 Average seasonality of midnight VOD at M34 compared with seasonality of leaf water concentration estimated from leaf demography data.

Notes S1 Additional model description for ED-2.2-hydro.

Table S1 Key plant photosynthetic, structural, and hydraulic traits for the three tree plant functional types (PFTs) used in our simulations.

Please note: Wiley Blackwell are not responsible for the content or functionality of any Supporting Information supplied by the authors. Any queries (other than missing material) should be directed to the *New Phytologist* Central Office.

See also the Commentary on this article by Gerlien-Safdi, **231**: 5–7.